ORIGINAL ARTICLE

lajss.org
Latin American Journal of Solids and Structures

www.lajss.org

An Anchorage System for Enhanced Bond Behavior between Carbon Fiber Reinforced Polymer Sheets and Cracked Concrete

Rami H. Haddad[a]*

[a] Jordan University of Science and Technology, P.O. 3030, 22110 Irbid, Jordan. E-mail: rhaddad@just.edu.jo

*Corresponding Author

https://doi.org/10.1590/1679-78255708

Abstract

The contribution of CFRP wraps, as an anchorage system, to enhancing bond behavior between CFRP sheet and cracked concrete, was investigated. Thirty six concrete blocks (150 x 150 x 200 mm) were cast with 3φ12 mm steel bars embedded laterally at different spacing along the 200-mm-dimension. Half of the moist-cured blocks were subjected to a cyclic treatment in 3% chloride solution until reinforced sides cracked at an average global crack size 0.54 mm; the remaining ones were immersed in a lime solution for a similar period, as controls. Finally, the blocks were attached at their reinforced surface to CFRP sheets at different bond widths and lengths with CFRP wrap anchorages applied over portions where high shearing stresses persist during pull-off testing. The results indicate that the physical status of concrete, the geometry of main CFRP sheets, and the extension of CFRP wrap anchorage are major factors that shape the benefit from the proposed anchorage technique. Empirical models, developed to predict bond strength and slippage at ultimate stress, show very good predictability of literature data.

Keywords

Anchorage, Corrosion cracks, Bond failure, Bond characteristics, Pull-off specimens.

1 INTRODUCTION

Exposure of concrete structures to salt contamination in marine environments or through intrusion of deicing chemicals stimulates corrosion of embedded steel reinforcement leading ultimately to the cracking of the surrounding concrete. The damage is caused by a hoop pressure generated by the transformation of superficial steel substrates into rust of much lower density (Neville, 1995). Flexural elements are the most susceptible to steel corrosion activity because their horizontal alignment allows easy intrusion of contaminating chemical. Active reinforcement corrosion in such structural members is usually associated with tangible reduction in the diameters of the reinforcing bars and undesirable changes in their surface and mechanical characteristics (Neville, 1995). These are accompanied with progressive concrete cracking along and across the concrete's cover over corroding reinforcement. Ultimately, structural elements lose its flexural and shear capacity as well as their resistance to various types of external attacks. Hence, repair procedure would be urgently needed to preserve structural integrity and prevent possible catastrophic failures (Sun at al., 2015; Yu et al. 2015; Song and Yu, 2015; Almassri et al., 2015; Azam and Soudki, 2013).

In field, several repair methods were used to recover the structural capacity of flexural members such as concrete jacketing, and attachment of steel plates or fiber reinforced polymer composites to the highly stressed proportions of these elements (Jones et al., 1988; Hussain at al., 1995; Haddad et al., 2008a; Haddad et al. 2008b). This is preceded by the removal of the cracked concrete cover; especially in repair cases associated with reinforcing steel corrosion. Available field statistics show that high percentage of replaced concrete covers in flexural elements undergoes cracking shortly after casting or whenever the rehabilitation utilized initially was ineffective in slowing down or preventing

Received: June 28, 2019. In Revised Form: August 05, 2019. Accepted: August 08, 2019. Available online: August 12, 2019.
http://dx.doi.org/10.1590/1679-78255708

Latin American Journal of Solids and Structures. ISSN 1679-7825. Copyright © 2019. This is an Open Access article distributed under the terms of the Creative Commons Attribution License, which permits unrestricted use, distribution, and reproduction in any medium, provided the original work is properly cited.

concrete deterioration (Sun at al., 2015; Song and Yu, 2015; Almassri et al., 2015; Azam and Soudki, 2013). Fire and durability attacks on repaired flexural elements along with drying shrinkage can cause further cracking of existing or newly replaced concrete surfaces (Al-Rousan at al., 2013; Haddad et al., 2013; Haddad and Al-Rousan, 2016; Siad et al., 2017; Aiello et al., 1999).

Various literature works show noticeable enhancement in the mechanical performance of the cracked reinforced concrete flexural elements upon repair using externally-bonded carbon fiber reinforced polymer (CFRP) sheets (Song and Yu, 2015; Almassri et al., 2015; Azam and Soudki, 2013). However, presence of cracking may lead to premature debonding of externally attached composites which undermines repair efficiency with CFRP (Khorramabadi and Burgoyne, 2011). In fact, Haddad and Al Dalou (2017) show that corrosion-induced cracks with sizes of 0.20 to 0.90 mm lead to significant degradation in bond performance between CFRP sheets and cracked concrete. The study also reveals that concrete-CFRP bond becomes more susceptible to corrosion cracks as bond width and length of the attached CFRP sheets are increased. Research attempts were made to examine the efficiency of using various anchorage techniques to improve CFRP-concrete bond behavior or minimize its degradation once concrete is cracked. These included the use of steel hooks, bolted steel plates, end FRP fans, and U-wrap FRP sheets, (Yoshitake, 2009; Biacaia et al., 2018; Xiang et al., 2013; Zhang and Smith, 2011). Haddad and Al-Rousan (2016) examined the feasibility of using varying lengths of CFRP wraps to end anchor CFRP plates, attached to heat-damaged normal and lightweight aggregate concrete blocks. Their findings indicate improved bond characteristics for thermally shocked and anchored pull-off specimens.

2. PROBLEM STATEMENT, OBJECTIVES AND SCOPE

The efficiency of using fiber reinforced polymer (FRP) composites in repairing/strengthening cracked flexural elements is doubtful because of the negative impact of induced cracks upon FRP-concrete's bond behavior (Haddad and Al Dalou, 2017). Since the detachment of the carbon fiber reinforced polymer (CFRP) composites from the flexural members initiates at regions of high tensile stresses towards the supports. The attachment of CFRP wraps on the top of CFRP reinforcement at these regions can potentially reduce the shearing stress concentration at concrete-CFRP interface, as illustrated in the schematic of Figure 1. Consequently, bond failure will be delayed or prevented while the benefit from strengthening becomes magnified. In this work, the contribution of single layers of CFRP wraps as an anchorage of main CFRP reinforcement is studied with emphasis placed upon the anchorage length of CFRP wraps, and the geometric characteristics of main CFRP sheets. Bond behavior is evaluated using pull-off specimens, assembled using control and cracked concrete blocks. The schematic of Figure 2 demonstrates how anchorage is applied to one of the two sides of present pull-off specimens.

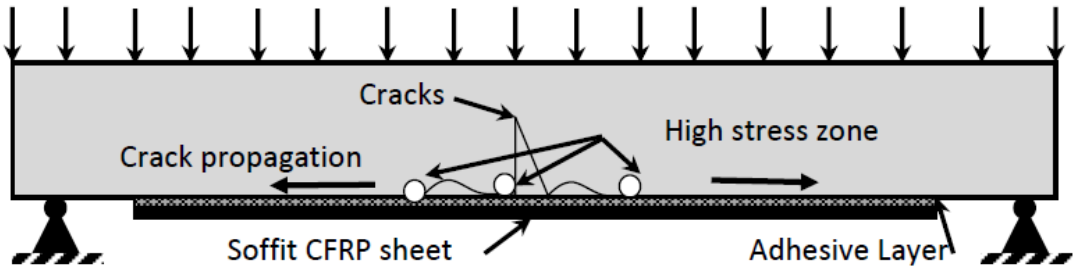

Figure 1: A schematic of a common case of CFRP detachments from strengthened concrete beams.

Thirty six concrete blocks (150x150x200 mm^3) were reinforced with φ12 mm deformed steel bars (spaced at 30–50 mm along the blocks longest dimension) before cast in wooden molds then cured for 28 days using wet burlap. Several factors were considered in selecting the dimensions of the present blocks including the geometric dimensions of the testing machine, presence of reinforcement at a concrete cover of 15 mm, and the ranges for bond widths and lengths for CFRP sheets. Eighteen of these blocks were subjected to a special treatment in a chloride solution for a period of 90 days to generate corrosion cracks at a global width of 0.54 mm, whereas the remaining identical ones were left for similar periods in lime water as controls. CFRP sheets of varying bond lengths (90 and 120 mm) and widths (50 and 100 mm) were adhered to these blocks on their steel reinforced side (150x200 mm^2) and the opposite ones using the proper epoxy. CFRP anchorage wraps were attached on the top of the main CFRP sheets at a constant width of 150 mm and variable lengths relative to that of the main CFRP sheets of (1/3 and 2/3), as shown in Figure 2. A letter-number designation was used to define both anchorage and repair configuration for control and corrosion damaged

specimens. For example, letters W, L, CR, and A in designation W5-L9-CR-A (0.67Lf) refer to bond width and bond length of CFRP sheets, corrosion cracked blocks, and anchorage, respectively. The fraction within brackets reflects the ratio of length of CFRP anchorage wraps to that of CFRP sheets, Lf. The geometric configurations of different specimens tested in the present work and their designations are summarized in Table 1.

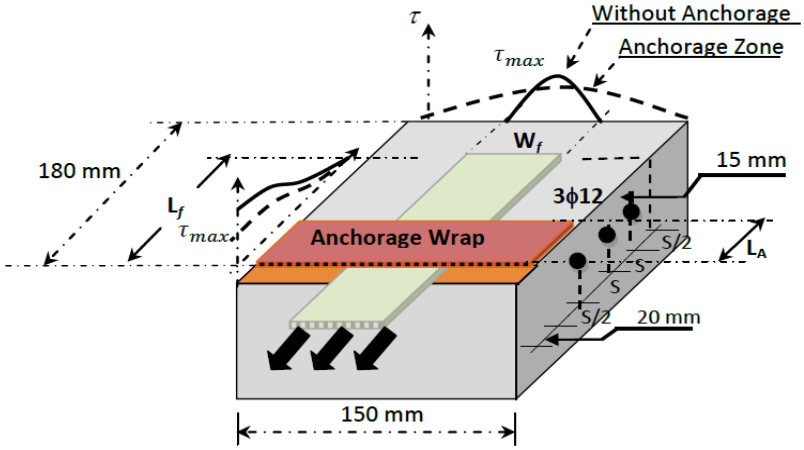

Figure 2: A schematic of pull-off specimens showing the CFRP sheet and the proposed anchorage wrap configuration.

Table 1: Designation of pull-off specimens used in present work.

Specimen Designation	Status	W_f	L_f	$\frac{L_A}{L_f}$
		mm	mm	
W10-L12-UC	UC	100	120	NA
W10L12-UC-0.33L_f	UC	100	120	0.33
W10L12-UC-0.67 L_f	UC	100	120	0.67
W10-L12-CR	CR	100	120	NA
W10L12-CR-0.33 L_f	CR	100	120	0.33
W10L12-CR-0.67 L_f	CR	100	120	0.67
W5L12-UC	UC	50	120	NA
W5L12-UC-0.33 L_f	UC	50	120	0.33
W5L12-UC-0.67 L_f	UC	50	120	0.67
W5L12-CR	CR	50	120	NA
W5L12-CR-0.33 L_f	CR	50	120	0.33
W5L12-CR-0.67 L_f	CR	50	120	0.67
W5L9-UC	UC	50	90	NA
W5L9-UC-0.33 L_f	UC	50	90	0.33
W5L9-UC-0.67 L_f	UC	50	90	0.67
W5L9-CR	CR	50	90	NA
W5L9-CR-0.33 L_f	CR	50	90	0.33
W5L9-CR-0.67 L_f	CR	50	90	0.67

UC: Uncracked, CR: Corrosion cracked, W_f: Bond width, L_f: Bond length, L_A / L_f : anchorage length to bond length ratio.

Simulation of actual distributions of cracking in concrete flexural elements in this study is impractical. Hence, we decided to consider only the impact of the cracks that are oriented in a direction perpendicular to that of CFRP fibers. Furthermore, a relatively low concrete cover of 15 mm from concrete surface was utilized in different concrete blocks to guarantee achieving tangible concrete cracks at the top of the corroding bars. Bond behavior was later evaluated using a special setup designed to force the de-bonding of the CFRP sheets from the cracked concrete substrate, as shown by the schematic of Figure 3. With such testing setup, the concrete underneath the CFRP sheets would be free to elongate during pullout testing simulating the stress conditions that predominates between loaded concrete beams

and CFRP composites, externally attached to promote flexural capacity. The obtained data was analyzed to establish the contribution of the proposed anchorage system to bond behavior of pull-off specimens.

3. TESTING PROCEDURE

3.1 CONCRETE MIXTURE AND REINFORCING STEEL

All concrete blocks were cast using same concrete mixture, designed to achieve a compressive strength of about 32 MPa and a slump in the range of 30-40 mm according to ACI mix design methods (ACI Manual of Concrete Practice, 2008). Drinking water, Type I Portland cement, coarse aggregate, fine limestone aggregate, and silica sand were mixed in a rotary mixer for 2 minutes at proportions of 210, 370, 846, 580, and 249 kg/m3, respectively, with a commercially available superplasticizer added at a dosage of 37 kg/m^3 to improve workability (ASTM, 2004). The physical properties of the aggregate particles were obtained according to ASTM testing methods [23]. The (bulk specific gravity (SSD) and absorption) for coarse and fine limestone and silica sand were (2.56 and 2%), (2.63 and 1.30%), and (2.59 and 0.80%), respectively. The fineness modulus for fine limestone and silica sand were 3 and 1.7, respectively. The unit's weight of coarse limestone was found to be 1500 kg/m^3. Concrete blocks were cast by placing concrete in two layers; each compacted by a vibrating table before their surfaces were finished smooth by a trowel. Standard cylinders (100x200 mm^2) were also cast by placing concrete at three layers during vibration. All specimens were unmolded after 24 hours of moist curing then covered with wet burlap to cure for another 27 days.

Steel bars at a diameter of 12 mm were used in reinforcing the present concrete blocks. The mechanical properties of these bars were obtained experimentally using a universal testing machine. The ultimate and yield tensile strengths were found to be 580 and 425 MPa, respectively.

3.2 CFRP COMPOSITES

CFRP sheets of unidirectional continuous fibers from BASF were used at different widths and lengths for assembling different pull-off specimens. Their elastic modulus, ultimate tensile strength, and ultimate strain capacity (as provided by the manufacturer) were 230 GPa, 4.9 GPa, and 2.1%, respectively. BASF adhesive was used for attaching the CFRP sheets to concrete according to the manufacturer's instructions. The adhesive tensile yield strength, tensile elastic modulus, bond strength and tensile rupture strain (as provided by the manufacturer) were 54 MPa, 3.034 GPa, 2.5 MPa, and 3.5%, respectively.

3.3 INDUCING CRACKS IN CONCRETE BLOCKS

Matured concrete blocks were subjected to a special treatment in 3% sodium chloride solution for 2 days then drying for another 3 days using a conditioning unit. The adopted treatment regime aimed at accelerating the corrosion of steel bars for inducing a specific crack width on the top of these bars. Wetting and drying cycles were carried out under a constant temperature of 40°C for a period of 90 days using the treatment chambers of Figure 3. The reasonably small size of present modified test specimens allowed carrying out corrosion cyclic treatment for different specimens at the same time, saving on experimental effort and time.

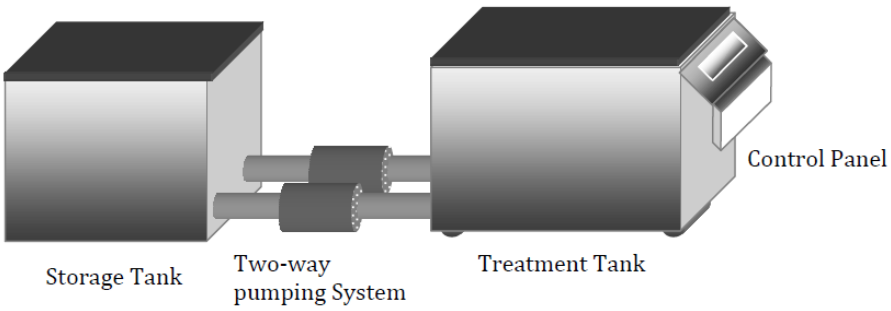

Figure 3: A schematic of chambers used to crack concrete through accelerating reinforcing steel corrosion.

3.4 ATTACHMENT OF CFRP SHEETS

A mechanically operated wire brush was used to remove cement's laitance, loose and friable material from the reinforced steel concrete face and the opposite side of the blocks before drying using methanol to reduce the

moisture's content. CFRP sheets of desired dimensions were then attached to the reinforced concrete face with and without anchorage wrap sheets. To ensure bond failure at this face, the CFRP sheets were attached at the opposite side at a length of 180 mm before being anchored with another sheet over the entire surface area. To install CFRP sheets, the correct adhesive form BASF was applied at an amount of 0.70 kg/m^2 to concrete or CFRP surfaces (where anchorage sheets were used) and at an amount of 0.50 kg/m^2 at the final surface of the CFRP sheets. Each installed sheet was rolled over until the adhesive was squeezed out to their top surface. The specimens were left in laboratory air for seven days to allow the adhesive to develop its ultimate adhesion strength. It is expected that small size cracks, underneath the CFRP sheets, would be closed partially or fully by the adhesive that is spread on concrete surface prior to the attachment of CFRP sheets. The various steps leading to the assembling of the present pull-off specimens using the concrete blocks (described earlier) are illustrated in pictures of Figure 4.



Figure 4: Assembling of the pull-off specimens: (a) preparing the surface of concrete blocks (left-top); (b) taping the borders of the bonding area (right-top); (c) applying of adhesive and rolling of CFRP sheets (left-bottom); (d) curing of pull-off specimens in air (right-bottom).

3.5 TEST SETUP

A testing setup was designed and fabricated to obtain bond force versus slip relationship for different pull-off specimens, as shown in Figure 5(a). A pull-off force was imposed by a universal testing machine at a loading rate of 200N/second until debonding failure between present concrete blocks and the CFRP sheets occurred, as shown in Figure 5(b). The mechanism adopted in testing allowed concrete in the blocks to elongate as the CFRP sheets were pulled-off. As shown, the pull-off force is transferred to CFRP sheets through 150-mm-diameter aluminum cylinder, pin-connected to a special frame that was tightly gripped to the upper head of the testing machine.

A Linear Variable Differential Transducers (LVDT) was used to measure onset slippage between concrete and the CFRP sheets, externally attached to the steel reinforced side of the blocks. For this, the LVDT was clamped by a small fiberglass holder, adhered on the top of the CFRP sheets, while its knob was in touch with another fiberglass prism, affixed to concrete surface. A data acquisition system was used to acquire pull-off force versus onset slippage readings.

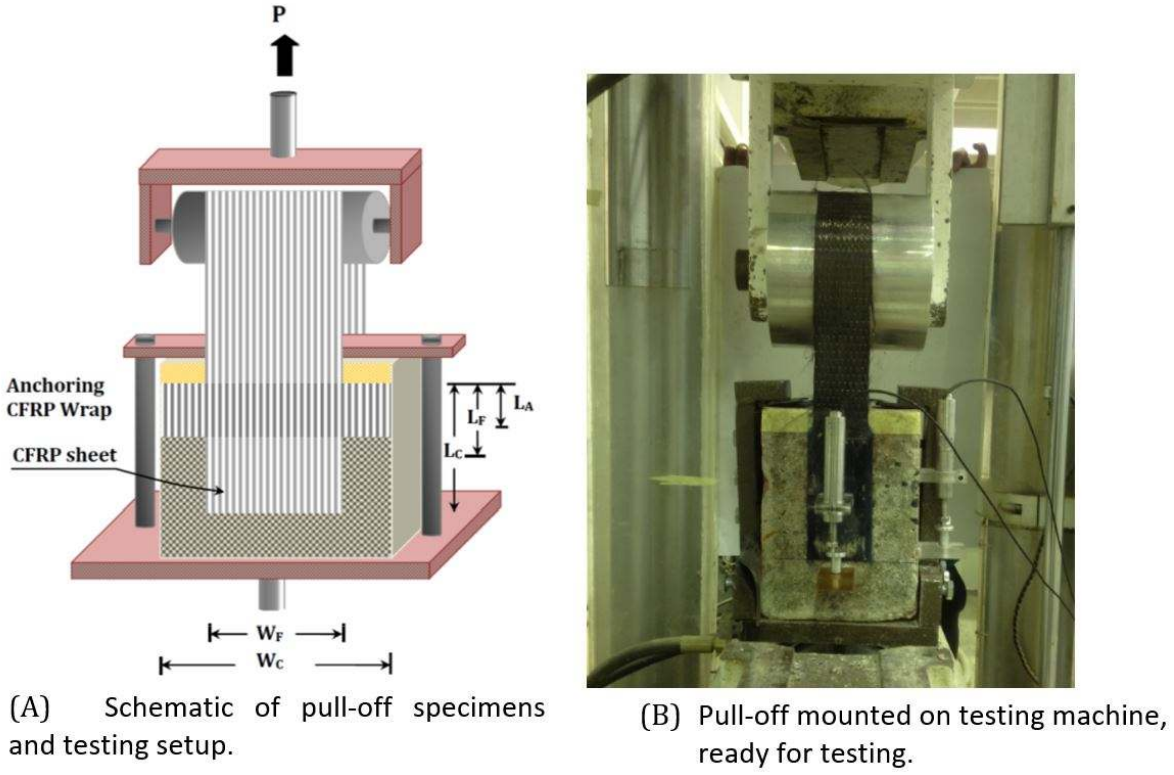

(A) Schematic of pull-off specimens and testing setup.

(B) Pull-off mounted on testing machine, ready for testing.

Figure 5: Configuration of pull-off specimens and testing setup.

4. RESULTS AND DISCUSSION

4.1 DAMAGE DUE TO REINFORCING STEEL CORROSION

Visual observation of corroded concrete blocks reveals that cracks initiated and propagated parallel to one or more of the reinforcing steel bars distributed laterally along the blocks largest dimension of 200 mm. The formation of these cracks is attributed to radial pressure generated by the transformation of exterior steel layers on the reinforcing bars into rust of much lower density (Wanga et al., 2016; Bassuoni and Rahman, 2016). Crack widths were measured using an optical microscope with an accuracy of 0.02 mm at six to nine points along the concrete cover above the reinforcing bars. The average crack width (ACW) was computed based on 12 to 18 readings from two concrete blocks of the same reinforcement configuration. The results of these readings were close to each others. For the present stage of corrosion, the ACW varied according to the spacing between the steel bars from 0.52 to 0.60 mm with a standard deviation of 0.03 for specimens (Shi et al., 2011). A global crack width (GCW) was computed at 0.56 mm and adopted as an indicator of the current corrosion damage level.

The percentage weight loss of corroded steel bars was evaluated for different corroded bars from different blocks. The corroded bars were cleaned using a commercial rust removing liquid before their weight loss computed with respect to original masses. The global weight loss after 90 days of treatment in chloride solution averaged at 3.8%. Corrosion damage was also evaluated using ultrasonic pulse velocity (UPV) technique. The lag time for an ultrasonic wave was measured for different concrete blocks before and after exposure to corrosion accelerating process according to ASTM test method C 597 (ASTM, 2004). Accordingly, a damage index, in terms of UPV, DIUPV, was computed using equation (4.1). The latter was increased significantly after 90 days of treatment in the chloride solution to 24% due to the noticeable increase in cracks width and extension across the depth of the present concrete blocks.

$$DI_{UPV} = 1 - \left(\frac{UPV_{Cracked}}{UPV_{Control}} \right)^2 \tag{4.1}$$

4.2 CFRP-CONCRETE BOND

The contribution of the proposed anchorage system to enhancing bond behavior between CFRP sheets and concrete is discussed in detail considering bond stress-slip relationship and its characteristics. Parameters considered include the CFRP attachment characteristics (bond length and width), and anchorage level.

4.2.1 BOND STRESS-SLIP RELATIONSHIP

The bond behavior of control and corroded pull-off specimens, prepared at varying bond widths and lengths of CFRP sheets, can be understood through Figs. 6–8. The curves presented were obtained by nonlinear fitting of the load-slip data pertaining to two identical specimens whose results were very close. As shown, the different curves follow a common trend represented in linear portions up to 50% of ultimate bond stress followed by a single concave down nonlinear portion for specimens without end anchorage, yet two nonlinear portions of reversed concavity for those with end anchorage. Generally, the point of inflection for the reversed curves corresponds to the ultimate load capacity of the identical specimens without anchorage. A different behavior would prevail if the CFRP anchorage wrap were to be adhered at the free-end instead of the loaded end of the main CFRP sheets. In such a case, the slippage at inflection point between the two nonlinear portions of the bond stress-slip curves matches ultimate slippage for identical specimens without anchorage (Haddad and Al-Rousan, 2016). The characteristics of the present bond stress-slip relationships of Figure 6–8 (ultimate bond stress, ultimate slippage, bond stress at slippage, bond stiffness and bond toughness) were computed before listed in Table 2.

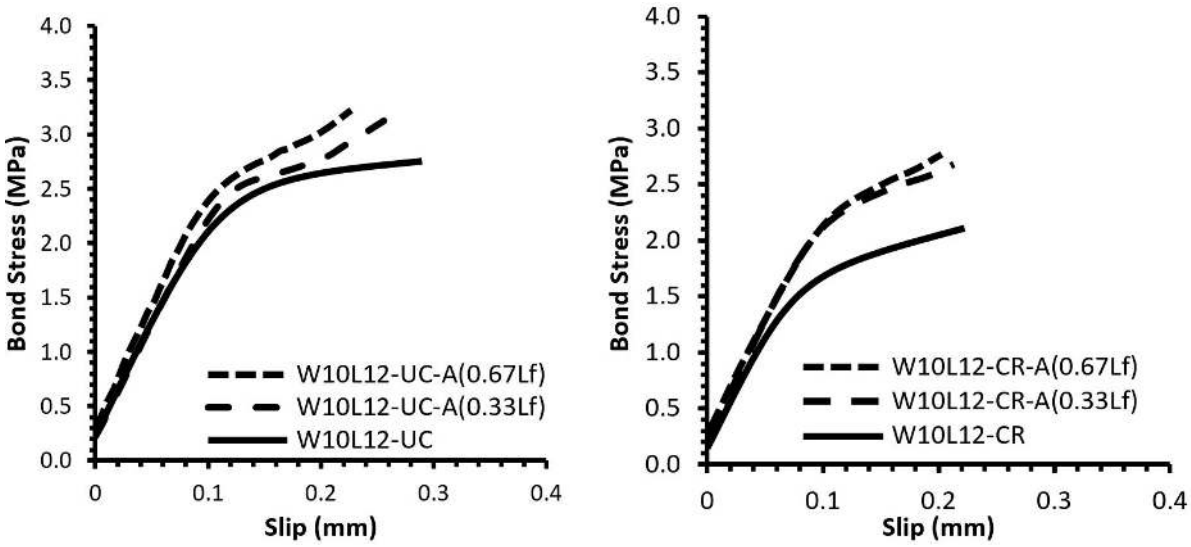

Figure 6: Bond stress versus slip for pull-off, assembled using control (left) and corrosion cracked (right) concrete blocks (bf=100 mm; Lf=120mm).

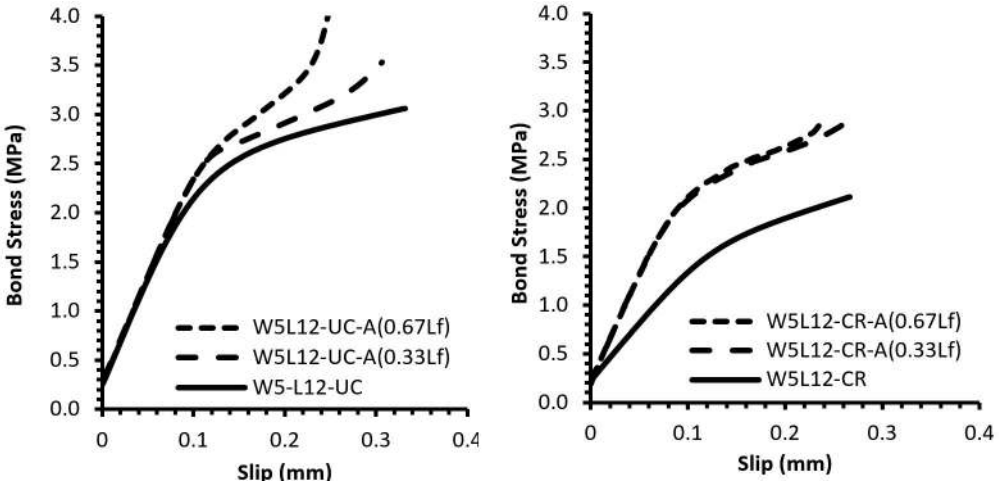

Figure 7: Bond stress versus slip for pull-off, assembled using control (left) and cracked (right) concrete blocks (b_f=50 mm; L_f=120mm).

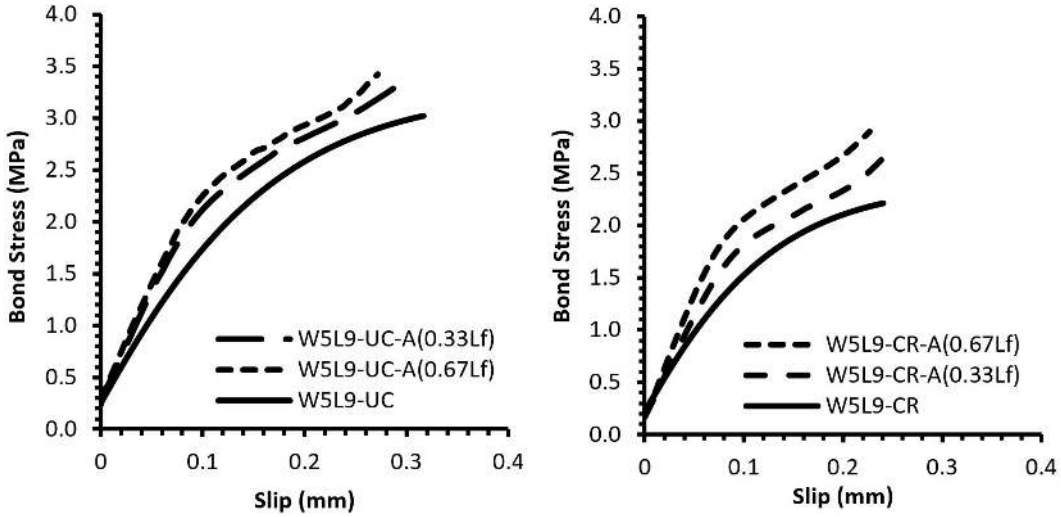

Figure 8: Bond stress versus slip for pull-off, assembled using control (left) and cracked (right) concrete blocks (bf=50 mm; Lf=90mm).

4.2.2 BOND CHARACTERISTICS

The results of Table 2 indicate clearly that bond strength, and bond stress at slippage were increased reaching 137 and 184% whereas slippage at ultimate stress and bond toughness were reduced to as low as 75 and 39%, respectively, when anchorage sheets were applied to portions of CFRP sheets where high shearing stresses persist during pull-off testing. On the other hand, bond stiffness was slightly affected by the application of the present anchorage regime. As can be deduced from Table 2, the residual for bond characteristics are dependent upon anchorage level, physical status of the concrete blocks (intact versus corrosion damaged) as well as bond length and width of main CFRP sheets, as discussed below.

Anchorage levels: The contribution of anchorage level upon residual bond characteristics is affected by the geometric characteristics of CFRP sheets as well as the physical status of concrete blocks. In general, extending anchorage length from 1/3 to 2/3 relative to bond length of the CFRP wraps contributes to higher improvements in bond characteristics between CFRP sheets and corrosion damaged blocks as compared to those between CFRP sheets and intact concrete blocks. Furthermore, the present results reveal that using CFRP anchorage wraps at higher extension is more beneficial when applied to main CFRP sheets of higher bond length yet lower bond width.

Physical status of concrete: The results of Table 2 indicate that the benefit from anchoring CFRP sheets over their high shearing stress zone is higher for corrosion-damaged than intact specimens. For example, the percentage increases in bond strength upon use of CFRP wraps to anchor CFRP sheets of bond length and width of (120 and 100 mm), (120 and 50mm), and (90 and 50 mm) were 15, 37, and 19% for pull-off specimens with intact blocks as compared to 29, 43, and 36% of those with corrosion damaged blocks. The residuals for slippage at ultimate stress and bond toughness show lower decrease upon anchorage for corrosion damaged blocks as compared to that for intact ones. As can be deduced, the differences between the residuals of bond characteristics for pull-off specimens with corrosion damaged and intact concrete blocks is slightly affected by the anchorage levels.

Geometric characteristics of CFRP sheets: The anchorage efficiency improved in terms of bond strength, stiffness, toughness, and slippage at ultimate stress as bond length increased from 90 to 120 mm with bond width kept constant at 50 mm. The behavior observed in Table 2 can be attributed to the longitudinal redistribution in shearing stress underneath the CFRP sheets through the high shear zone where anchorage was applied, as illustrated in the schematic of Figure 1. Hence, the efficiency of anchorage was enhanced further for pull-off specimens at higher bond length where deviation between extreme shearing stresses at the CFRP-concrete interface becomes greater (Subramaniam et al., 2007).

As expected, the present anchorage system imparted higher improvement to bond characteristics for CFRP sheets at the lower bond width of 50 mm as compared to that 100 mm, especially for specimens assembled using intact concrete blocks. This is referred to that the present CFRP anchorage wraps, applied across the full width of the concrete blocks, worked on redistributing shearing stresses, hence imparted higher resistance against CFRP sheets detachment, as clarified in the schematic of Figure 2 (Subramaniam et al., 2007).

Table 2: Bond characteristics and failure modes for different pull-off specimens without and with anchorage using CFRP bandages.

Specimen Designation	UPL	τ_{max} kPa	S_o	BSS	BST GPa/m	BT	FM
	kN		µm	kPa		J/m²	
W10-L12-UC	33.93	2828	291.7	0.254	21	618	CSP
	100*	100	100	100	100	100	
W10L12-UC-0.33L_f	37.76	3147	255.8	0.227	20.2	261	CSP
	111	111	88	89	96	42	
W10L12-UC-0.67L_f	39.05	3254	226.9	0.306	20.5	240	CSP
	115	115	78	120	98	39	
W10-L12-CR	26.19	2183	217.2	0.149	19.7	345	CSP
	100	100	100	100	100	100	
W10L12-CR-0.33L_f	33.81	2818	227.5	0.235	20.2	194	CCP
	129	129	105	158	102	56	
W10L12-CR-0.67L_f	33.76	2813	203	0.274	19.4	187	CCP
	129	129	93	184	98	54	
W5-L12-UC	18.78	3130	337.4	0.259	21.4	771	CSP
	100	100	100	100	100	100	
W5L12-UC-0.33L_f	22.23	3705	306.6	0.267	21.6	351	CSP
	118	118	91	103	101	46	
W5L12-UC-0.67L_f	25.76	4293	251.8	0.256	20.7	465	CSP
	137	137	75	99	97	60	
W5-L12-CR	13.09	2182	275.1	0.232	13.8	384	CSP
	100	100	100	100	100	100	
W5L12-CR-0.33L_f	18.73	3122	274.2	0.194	22.5	244	CSP+AS
	143	143	100	84	163	64	
W5L12-CR-0.67L_f	17.91	2985	239.5	0.24	20.7	225	CSP+AS
	137	137	87	103	150	59	
W5L9-UC	13.59	3020	316	0.25	17.6	655	CSP
	100	100	100	100	100	100	
W5L9-UC-0.33L_f	15.54	3453	293.1	0.235	21.3	322	CSP+AS
	114	114	93	94	121	49	
W5L9-UC-0.67L_f	16.17	3593	271.8	0.287	21.1	315	CSP
	119	119	86	115	120	48	
W5L9-CR	9.95	2211	240.4	0.185	17.2	367	CSP
	100	100	100	100	100	100	
W5L9-CR-0.33L_f	12.01	2669	246.2	0.168	19.1	238	CSP+AS
	121	121	102	91	111	65	
W5L9-CR-0.67L_f	13.55	3011	226.7	0.187	21.4	227	CSP+AS
	136	136	94	101	124	62	

*, Residual characteristics with respect to uncorroded pull-off specimens ; UPL, Ultimate pull-off load; τ_{max}, bond strength; S_0, Slippage at ultimate stress; BSS, Bond stress at slippage; BST, Bond stiffness; BT, Bond toughness; FM, Failure mode; CSP, Concrete skin peeling-off; AS, anchorage shearing-off; CCP, concrete cover peeling-off.

4.2.3 BOND FAILURE MODES

The present testing setup allows the concrete in contact with CFRP sheets to elongate as the universal testing machine head is displaced further. This caused the corrosion-created cracks to open further, creating high stress concentration underneath and in the vicinity of the main CFRP sheet which led to the premature failure of pull-off specimen, especially those prepared with corrosion-cracked specimens. CFRP anchorage wraps were effective in delaying bond failure and led to modifications in the failure mode between CFRP composites and concrete.

As summarized in Table 2, skin peeling-off failure was dominant for different specimens except for corrosion cracked specimens, assembled at bond width and length of 100 and 120 mm, respectively, where concrete cover detachment mode was identified. This occurred because corrosion cracks, extended at the level of steel, causing concrete cover peeling-off at a lower pull-off force of that needed to cause failure by concrete skin peeling-off. Failure

modes indicate higher thickness of detached concrete for corrosion damaged than for control blocks with shearing-off in anchorage wraps for the cases involving the use of relatively low bond width and length of CFRP sheets. Hence, it is recommended to use two 90-degree ply layers of CFRP anchorage wraps in future investigations.

5. EMPIRICAL MODELING OF BOND STRENGTH AND SLIPPAGE

The above discussion reveals that the contribution of the present anchorage system to bond characteristics is shaped by different interacting factors namely, geometric configuration of main CFRP sheet, physical status of concrete, and anchorage level. In this part, empirical equations for the prediction of bond strength and slippage at ultimate stress are presented, and their accuracy of prediction examined using relevant data by (Haddad and Al Dalou, 2017). To validate further the present model (proposed for bond strength), its accuracy of prediction was compared to those of well-known literature models (Wu et al., 2012; Chen and Teng 2001; Lu et al., 2005). Literature data from different sources are used in the validation process (Al-Rousan et al., 2013; Haddad et al., 2013; Al-Rousan at al., 2014; Haddad et al., 2015).

Based on the trend behavior observed for bond stress versus slippage of Figures 6-8, two models are proposed for bond strength (τ_{max}) and slippage at ultimate bond stress (S_o) according to equations (1-2). These models are similar, in general form, to those by Lu et al. (2005). The models include parameters that account for degradation in bond behavior due to concrete cracking, geometry of repair using CFRP sheets, anchorage effect by CFRP wraps, and splitting strength of concrete. The geometric parameters are expressed in terms of bond length and width relative to concrete dimensions, L_f / L_C and b_f / b_C, respectively, according to equation (3) through (6), already developed by Haddad and Al Dalou (2018).

$$\tau_{max} = {}_{D,\tau}\ \tau_i + \alpha\ {}_{D,\tau L,w,}\beta_{A,\tau}\sqrt{f_c^{'}} \tag{1}$$

$$S_o = \alpha_{SD,SL,Sw,S}\beta_{A,S}\sqrt{f_c^{'}} \tag{2}$$

Where

${}_{\tau}$: Statistical coefficient (bond strength).

${}_{S}$: Statistical coefficients (slippage at ultimate bond stress).

${}_{D,\tau}$: Degradation parameter for bond strength

${}_{D,S}$: Degradation parameter for slippage at ultimate bond stress.

$\beta_{A,\tau}$: Anchorage parameters for bond strength

$\beta_{A,S}$: Anchorage parameters for slippage at ultimate bond stress.

$f_c^{'}$: Compressive strength of a standard concrete cylinder (MPa).

$\beta_{w,\tau}$: Geometric width (w) parameter relevant to bond strength.

$\beta_{L,\tau}$: Geometric length (L) parameter relevant to bond strength.

$\beta_{w,S}$: Geometric width (w) parameter relevant to slippage at ultimate bond stress.

$\beta_{L,S}$: Geometric length (L) parameter relevant to slippage at ultimate bond stress.

$$_{w,} = \sqrt{\frac{\left(2-\frac{b_f}{b_C}\right)}{\left(2.25+\frac{b_f}{b_C}\right)}} \tag{3}$$

$$_{L,}=\sqrt{\frac{\left(1.75-\frac{L_f}{L_C}\right)}{\left(2+\frac{L_f}{L_C}\right)}} \quad (4)$$

$$_{w,S}=\sqrt{\frac{\left(2.25-\frac{b_f}{b_C}\right)}{\left(2+\frac{b_f}{b_C}\right)}} \quad (5)$$

$$_{L,S}=\sqrt{\frac{\left(2+\frac{L_f}{L_C}\right)}{\left(2-\frac{L_f}{L_C}\right)}} \quad (6)$$

The degradation parameters $_{\mathrm{D},\tau}$ and $_{\mathrm{D,S}}$ were also related to global cracking width (GCW) and damage index in terms of ultrasonic pulse velocity (DIUPV) through linear regression according to equations 7–10 for the case without anchorage ($\beta_{A,\tau}$ and $\beta_{A,S}$ =1) (Haddad and Al Dalou, 2018). It is important to state that the combination of the latter parameters and the square root of the compressive strength for intact concrete, adopted in Equations (1–2), can be considered as a valid quantification of the physical status of concrete in lieu of the compressive strength for cracked concrete; practical evaluation of which was almost impossible. It was found that the degradation parameters for bond strength and slippage at ultimate stress range from (0.66 to 0.86) and (0.63 to 0.89), respectively. These are in agreement with values, recommended by ACI 440.7 for the design of repair for degraded reinforced concrete elements (ACI Committee 440, 2008).

$$_{D,\tau}=-0.012DI_{UPV}+1.004\le 1 \quad (7)$$

$$_{D,\tau}=-0.353GCW+0.963\le 1 \quad (8)$$

$$_{D,S}=-0.012DI_{UPV}+1.022\le 1 \quad (9)$$

$$_{D,S}=-0.389GCW+0.984\le 1 \quad (10)$$

The parameters that account for the effect of anchorage effect, $\beta_{A,\tau}$ and $\beta_{A,S}$, were obtained in the present study by linear fitting of equations (1-2) using the experimental bond data for the cases with and without wrap anchorage with geometric and degradation parameters computed according to equations (3-6) and (7-10), respectively. As indicated by Figures 9, the model fit of the present data can be rated as very good with a coefficient of determination (R^2) in excess of 0.83. The anchorage parameters obtained were then expressed in terms of anchorage length to the bond length for the CFRP sheets, L_A / L_f, bond length and width ratios relative to concrete dimensions, L_f / L_C and b_f / b_C, respectively, and degradation parameters relevant to bond strength ($_{\mathrm{D},\tau}$) and slippage at ultimate bond stress ($_{\mathrm{D,S}}$). The expression for $\beta_{A,\tau}$ and $\beta_{A,S}$ were formulated in terms of the above parameters, as indicated by equations (11-12).

$$\beta_{A,\tau} = e^{\left\{\frac{\left\{\left\{\sqrt{\frac{L_A}{L_f}}+1\right\}\frac{L_f}{L_C}\right\}}{\left\{2.5-\frac{b_f}{b_C}\right\}}\right\}^{\beta_{D,\tau}}} \tag{11}$$

$$\beta_{A,S} = \left\{\frac{2-\frac{b_f}{b_C}}{\sqrt{\frac{L_A}{L_f}}+\frac{L_f}{2L_C}+2}\right\}^{\frac{\beta_{D,S}}{2}} \tag{12}$$

The accuracy of prediction by the models of equations (1–2) were validated using bond data from tests on pull-off specimens with corrosion cracked blocks (Haddad and Al Dalou, 2017). These data were not used in the development of the present models. As can be deduced from Table 3, the error in prediction of bond strength and slippage at ultimate stress averaged at about 13 and 11% with standard deviations of approximately 10 and 7%, respectively. These indicate satisfactory model prediction of test data (Haddad and Al Dalou, 2017); regardless of the variation in the cracks width and distribution between concrete blocks, underwent similar corrosion level and prepared at different reinforcing steel spacing.

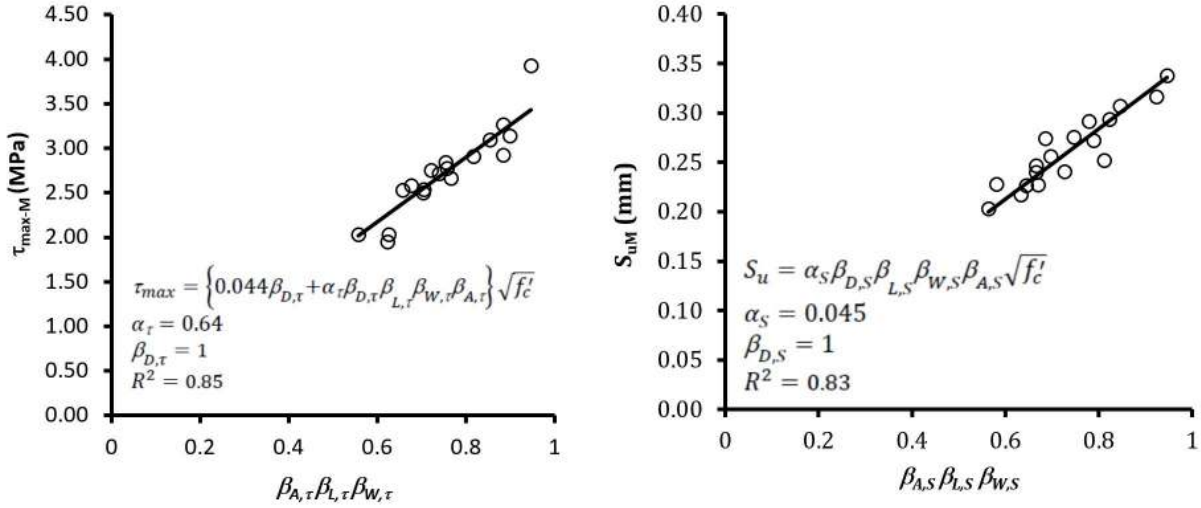

Figure 9: Linear fitting of the multiplication of anchorage, and geometric parameters versus bond strength (left) and slippage at ultimate stress (right).

Table 3: Measured and predicted bond strength and slippage at failure for control and corroded pull-off specimens without anchorage (Haddad and Al Dalou, 2017)

L_f	W_f	$\beta_{D,\tau}$	$\tau_{max\text{-}M}$	$\tau_{max\text{-}P}$	E	$\beta_{D,S}$	S_{uM}, mm	S_{uP}, mm	E
mm	*mm*		MPa	Pa	%				%
90	100	1	2.97	2.54	14.5	1	0.2701	0.2663	1.4
120	100	1	2.83	2.52	11	1	0.2917	0.2839	2.7
150	100	1	2.48	2.48	0.1	1	0.324	0.3041	6.1
120	50	1	3.1	2.81	9.3	1	0.3374	0.3734	10.7
120	150	1	2.24	2.54	13.3	1	0.2543	0.206	19
90	100	0.86	2.23	2.28	2.1	0.89	0.2255	0.2438	8.1
120	100	0.86	2.53	2.24	11.4	0.89	0.2603	0.2604	0
150	100	0.86	2.2	2.54	15.5	0.89	0.3023	0.2794	7.6

L_f	W_f	$\beta_{D,\tau}$	τ_{max} -M	τ_{max} -P	E	$\beta_{D,S}$	S_{uM}, mm	S_{uP}, mm	E
mm	*mm*		MPa	Pa	%				%
120	50	0.86	2.64	2.03	23	0.89	0.3067	0.3382	10.3
120	150	0.86	2.1	2.29	9.1	0.89	0.2243	0.1919	14.4
90	100	0.74	1.93	2.06	6.6	0.76	0.1813	0.2152	18.7
120	100	0.74	2.18	2.02	7.2	0.76	0.2172	0.2304	6.1
150	100	0.74	1.8	2.3	27.7	0.76	0.2413	0.2477	2.6
120	50	0.74	2.18	1.83	15.9	0.76	0.2751	0.2949	7.2
120	150	0.74	1.88	2.07	10.2	0.76	0.2093	0.173	17.3
90	100	0.66	1.74	1.91	9.5	0.63	0.156	0.1844	18.2
120	100	0.66	1.83	1.87	2	0.63	0.1635	0.1978	21
150	100	0.66	1.58	2.13	34.9	0.63	0.213	0.2132	0.1
120	50	0.66	1.75	1.69	3.2	0.63	0.2201	0.2497	13.4
120	150	0.66	1.68	2.28	35.6	0.63	0.1779	0.1514	14.9

L_f, bond length of CFRP sheet; W_f, bond width of CFRP sheet; τ_{max} -M, measured bond strength; τ_{max} -P, predicted bond strength; S_{uM}, measured slippage at failure; S_{uP}, predicted slippage at failure; $\beta_{D,\tau}$, degradation coefficient in bond strength; $\beta_{D,S}$, degradation coefficient in slippage at failure; E, error in prediction.

The potential of using the present model for future practical application is further established by comparing its accuracy of predictions to those of the models by Chen and Teng (2001) Wu et al. (2012) and Lu et al. (2005). These account for the effect of the geometric characteristics of CFRP sheets relevant to those of concrete and compressive strength of concrete but not the anchorage effect or the degradation in the physical status of concrete. Relevant literature data, not used in the model development, was used for this purpose. The test data was based upon pull-off testing of specimens, comprised from self-compacting, normal, and light weight concrete blocks that were attached to CFRP sheets using adhesives similar to those used in the present study (Al-Rousan et al., 2013; Haddad et al., 2013; Al-Rousan at al., 2014; Haddad et al., 2015). For the purpose of studying accuracy of prediction by the present model as compared to that of the different literature ones, degradation and anchorage parameters were set as ($\beta_{A,\tau}=1$) and $\left(L_A/L_f=0\right)$ equations (11-12), respectively.

Figures 10 show predicted bond strength (τ_{max-P}) versus measured bond strength (τ_{max-M}) for the different models. Only less than 10% of the predictions by the present model deviate slightly from the ideal prediction line, while those by other models tend to deviate significantly. As can be seen, the model by Lu et al. (2005) overestimates whereas that by Chen and Teng (2001) underestimates the bond strength between CFRP sheets and concrete. On the other hand, the model by Wu et al. (2012) provides predictions with large scattering around the ideal line. The bond strength ratio for each test point of Figure 9 was computed as predicted divided by measured value. This average ratio was computed for different models along with corresponding standard deviation then reported at the top of Figures 10. The average bond strength ratio and standard deviation for the present model are (0.91 and 0.23) as compared to (0.87 and 0.64), (0.66, 0.13), and (1.85, 0.41) for the models by Wu et al. (2012), Chen and Teng (2001), and Lu et al. (2005), respectively. These statistics show that the present model provides the best accuracy of predictions with limited deviation. It confirms previous conclusions regarding the performance of the literature models tested (Wu et al., 2012; Chen and Teng 2001; Lu et al., 2005).

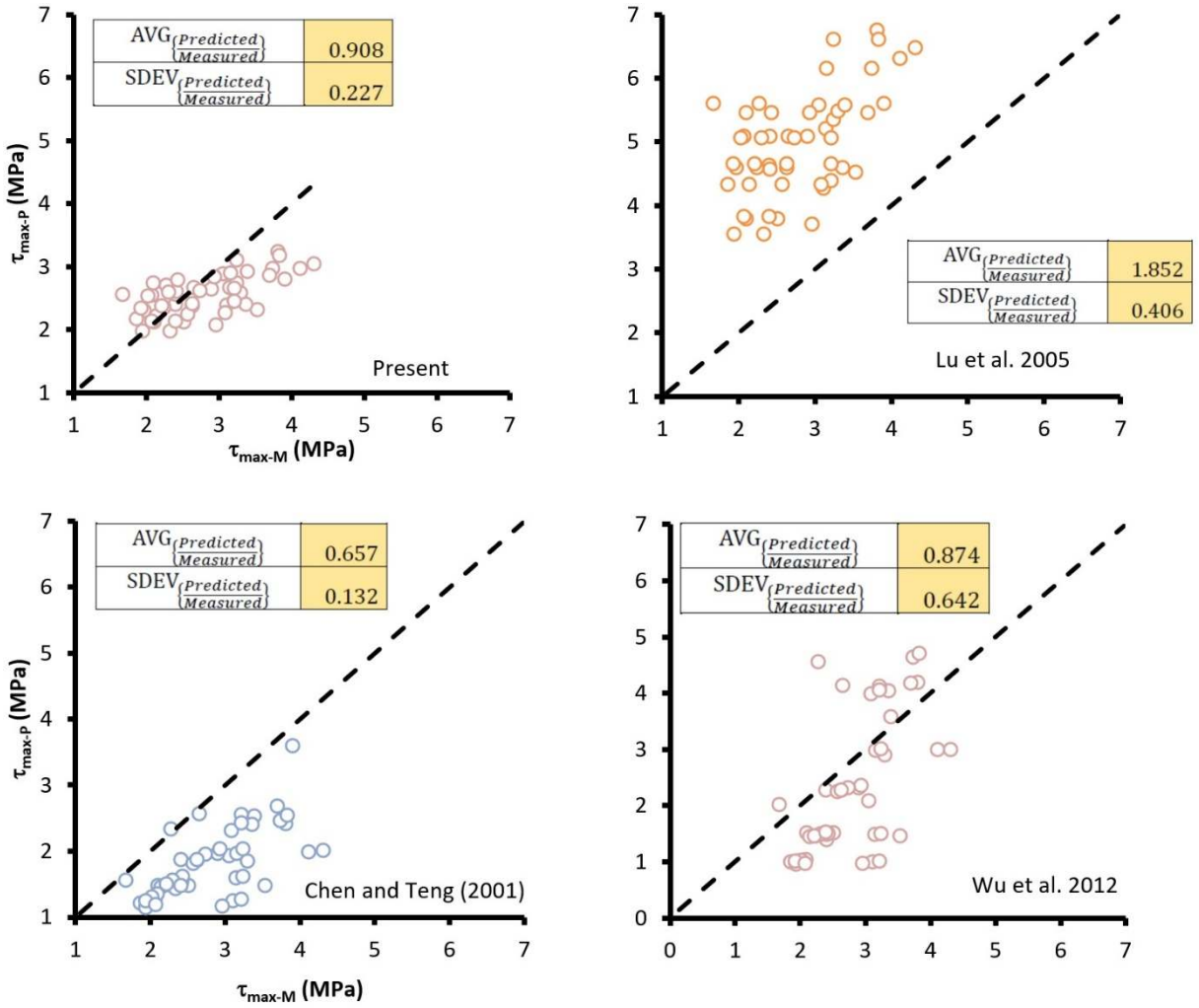

Figure 10: The Precision of bond strength predictions using present as compared to well-known literature models.

6. CONCLUSIONS

The following conclusions are extracted from the test results:

- Pull-off specimens, assembled using cracked concrete blocks and CFRP sheets at varying length and widths, show significant reduction in bond characteristics as compared to those of specimens with intact blocks. The percentage reductions in bond strength, bond stiffness, bond at slippage, slippage at ultimate stress, and bond toughness reach as high as 30, 36, 26, 41, and 50%, respectively.
- The bond stress-slip relationship of pull-off specimens without anchorage shows linear followed by nonlinear behavior until failure exhibited as concave down curves. On the other hand, those prepared with CFRP sheet anchorage experience double-reversed concavity in their nonlinear segments prior to failure.
- The benefit from applying the present sheet anchorage in enhancing bond strength is higher for pull-off specimens, assembled with corrosion cracked than intact blocks, especially for cases using higher bond lengths and widths of main CFRP sheets.
- Generally, the present anchorage lead to tangible reductions in slippage at ultimate stress and bond toughness with limited impact upon bond stiffness.
- Most of pull-off specimens with anchorage fail by concrete skin peeling coupled with shearing of anchorage wraps, except for some of those assembled with corroded blocks at relatively high attachments area of CFRP sheets, which show concrete cover peeling-off.

- The empirical models developed for predicting bond strength and slippage at ultimate stress took into consideration the effect of key parameters, discussed earlier. The predictions of the developed models show better precision than those of well-known literature models.

Acknowledgement

The authors acknowledge the technical and financial support provided by the research deanship at Jordan University of Science and Technology (project number 172/2015) and the assistant by the technicians at the structural and materials laboratory in the Department of Civil Engineering.

Author's Contributions: Conceptualization, RH Haddad; Methodology, RH Haddad; Investigation, RH Haddad; Writing - RH Haddad; Writing - review & editing, RH Haddad; Funding acquisition, RH Haddad; Resources, RH Haddad; Supervision, RH Haddad.

Editor: Marcílio Alves.

References

ACI Committee 440, (2008). Guide for the Design and Construction of Externally Bonded FRP Systems for Strengthening Concrete Structures, 440.2R-08 (PA, USA).

ACI Manual of Concrete Practice, (2008). Standard practice for selecting proportions for normal, heavyweight, and mass concrete (ACI 211.1), Part I: Materials and General Properties of Concrete (Michigan, USA).

Aiello, M., Focacci, F., Huang, P.C. Nanni, A. (1999) Cracking of Concrete Cover in FRP Reinforced Concrete Elements under Thermal Loads. 4th International Symposium on FRP for Reinforcement of Concrete Structures (FRPRCS4) (Baltimore, MD).

Almassri, B., Kreit, A., Al Mahmoud, F., Francois, R. (2015) Behavior of corroded shear-critical concrete beams repaired with NSM CFRP rods. Composite Structures 123: 204-215.

Al-Rousan, R., Haddad, R., Al-Halboni, A. (2014) Bond–slip behaviour between self-compacting concrete and carbon-fibre-reinforced polymer sheets. Magazine of Concrete Research 67(2): 89-103.

Al-Rousan., R., Haddad, R., Al-Sa'di, K. (2013) Effect of sulfates on bond behavior between carbon fiber reinforced polymer sheets and concrete. Materials and Design 43: 237-248.

ASTM, (2004). American Society for Testing and Materials International (PA, USA).

Azam., R., Soudki, K. (2013) Structural performance of shear-critical RC deep beams with corroded longitudinal steel reinforcement. Cement Concrete Composites 23: 946-957.

Bassuoni, M. T., Rahman, M. M. (2016). Response of concrete to accelerated physical salt attack exposure. Cement Concrete Research 79: 395–408.

Biacaia, H. C., Chastr, C. Silca, C., Franco, N. (2018). Mechanical response of anchored FRP bonded joints: A nonlinear analytical approach. Mechanics of Composite Materials and Structures 25(3): 238-252, 2018.

Chen, F., Teng, J. G. (2001). Anchorage strength models for FRP and steel plates bonded to concrete. Journal of Structural Engineering 127(7): 784–91.

Haddad, R. H., Shannag, M. J., Al-Hambouth, M. T. (2008a) Repair of reinforced concrete beams damaged by alkali-silica reaction. ACI Structural Journal 105(2): 145-153.

Haddad, R. H., Shannag, M. J., Moh'd, A. (2008b) Repair of heat-damaged shallow beams using advanced composites. Materials and Structures 41: 287-299.

Haddad, R., Al Dalou, A. (2017). Bond behavior between corrosion-cracked reinforced concrete and CFRP sheets. Journal of adhesion Science Technology 32(6): 590-608.

Haddad, R., Al Dalou, A. (2018). Modeling Bond Behavior between Corrosion-Cracked Reinforced Concrete and CFRP Sheets. Proceeding of the IRES - 435th International Conference on Innovative Engineering Technologies (ICIET), Antalya, Turkey.

Haddad, R., Al-Rousan, R. (2016). An anchorage system for CFRP strips bonded to thermally shocked concrete. International Journal of Adhesion and Adhesives 71: 10-22.

Haddad, R., Al-Rousan, R., Almasry, A. (2013) Bond-slip behavior between carbon fiber reinforced polymer sheets and heat-damaged concrete. Composites Part B 45(1): 1049-1060.

Haddad, R., Al-Rousan, R., Ganma, L., and Nimry, Z. (2015). Modifying CFRP-Concrete bond characteristics from pull-out testing. Magazine Concrete Research 67(13): 707-717.

Hussain, M., Sharif, A., Basunul, I. A. Baluch, M. H., Al-Sulaimani, G. J. (1995) Flexural behavior of precracked reinforced concrete beams strengthened externally by steel plates. ACI Structural Journal 92(1): 14–22.

Jones, R., Swamy, R. N., Charif, A. (1988) Plate separation and anchorage of reinforced concrete beams strengthened by epoxy-bonded steel plates. Structural Engineer 66(5): 85–94.

Khorramabadi, M., Burgoyne, C.J. (2011). Differences between FRP Bond Behavior in Cracked and Uncracked Regions. Fiber-Reinforced Polymer Reinforcement for Concrete Structures 10th International Symposium. ACI Special Publication SP-275: 335-351.

Lu, X., Teng, J., Ye, L., Jiang, J. (2005). Bond–slip models for FRP sheets/plates bonded to concrete. Engineering Structures 27(1): 920–937.

Neville, M. (1995). Properties of Concrete, 4th and final edition, Addison Wesley Longman Limited (England).

Shi, X., Yang, Z., Liu, Y. (2011). Cross D. Strength and corrosion properties of Portland cement mortar and concrete with mineral admixtures. Construction and Building Materials 25: 3245–3256.

Siad, A., Bencheikh, M., Hussein, L. (2017). Effect of combined pre-cracking and corrosion on the method of repair of concrete beams. Construction and Building Materials 132: 462–469.

Song, L., Yu, Z. (2015) Fatigue performance of corroded reinforced concrete beams strengthened with CFRP sheets. Construction and Building Materials 90: 99-109.

Subramaniam, K.V., Carloni, C., Nobile, L. (2007). Width effect in the interface fracture during shear debonding of FRP sheets from concrete. Engineering Fracture Mechanics 74: 578–594.

Sun, J., Huang, Q., Ren, Y. (2015). Performance deterioration of corroded RC beams and reinforcing bars under repeated loading, Construction Building Materials 96: 404-415, 2015.

Wanga, H. L., Dai, J. G., Sun, X. Y., Zhang, X. L. (2016). Characteristics of concrete cracks and their influence on chloride. Construction Building Materials 107: 216–225.

Wu, Y. F., Xu, X. S., Sun, J. B., Jiang, C. (2012). Analytical solution for the bond strength of externally bonded reinforcement. Composite Structures 94 (11): 3232–3241.

Xiang, L., Xiang, L.G., Xiao, B. S., Yu, O., Zhan, L. F. (2013). Contribution of U-shaped strips to the flexural capacity of low-strength reinforced concrete beams strengthened with carbon fiber composite sheets. Composite Part B 45(1): 117-126.

Yoshitake, E. (2009). Composite strips with various anchor systems for retrofitting concrete beams. International Journal Concrete Structures and Materials 5(1): 43-48.

Yu, L., Francois, R., Dang, V. H., L'Hostis, V., Gagne', R. (2015) Distribution of corrosion and petting factor of steel in corroded RC beams. Construction Building Materials 95: 384-392.

Zhang, W., Smith, T. (2011). Influence of FRP anchor fan configuration and dowel angle on anchoring FRP strips. Composite Part B 43 (8): 3516-3527.